



ALMA observations and radiative transfer modelling of low- and high-mass star-forming systems

R. Galván-Madrid¹ and A. F. Izquierdo²

¹ Instituto de Radioastronomía y Astrofísica (IRyA), UNAM, Apdo. Postal 72-3 (Xangari), Morelia, Michoacán 58089, Mexico, e-mail: r.galvan@irya.unam.mx

² Jodrell Bank Centre for Astrophysics, School of Physics and Astronomy, University of Manchester, Oxford Road, Manchester M13 9PL, UK

Abstract. We report on the user-friendly `SF3DMODELS` Python package originally released in Izquierdo et al. (2018), which is able to create complex 3D models in the context of star formation. These models are then plugged into radiative transfer codes such as `LIME`, `POLARIS`, or `RADMC-3D` to calculate synthetic images of their dust and free-free continuum, as well as their molecular and recombination line emission. We summarize the first two applications of these tools. i) In Izquierdo et al. (2018) we modelled ALMA observations of the massive YSOs in W33A MM1, an object previously interpreted as a single, massive disk in the pre-ALMA days, and that current data revealed is a multiple, complex system being fed by accretion streamers. ii) In Galván-Madrid et al. (2018) we investigated the effects of self-obscuration in class 0 protostellar disks, where we found that observed shallow (sub)mm spectral indices can be explained without invoking for very fast growth of dust grains. We also reproduce resolved images of dark lanes – “hamburguers” – in these YSOs when observed with the maximum resolution achievable with ALMA.

Key words. radiative transfer – stars: formation – stars: massive – stars: protostars

1. Introduction

Synthetic observations are becoming one of the most important tools to bridge the gap between raw theory and observations (e.g., Smith et al. 2016; Offner et al. 2011). We do not directly observe any astrophysical phenomena, but rather some of their tracers passed through an instrument response. In summary, one needs to have a physical model over which radiative transfer calculations are performed. Further steps such as passing the calculated model through the instrument response or model min-

imization are also desirable. Some very useful tools have been developed in the past to aid the interpretation of radio- and (sub)mm data (e.g., van der Tak et al. 2007), but the considered physical models are typically very simple.

With the advent of (sub)mm interferometry, high dynamic range observations at 0.01'' to 1'' resolution are now routinely performed. Those resolutions are equivalent to a physical resolution power of ~ 1 to 100 au in nearby, low-mass star formation regions, or to $\sim 10^1 - 10^3$ au in sites of high-mass star formation at kpc distances. Furthermore, synthesis-imaging

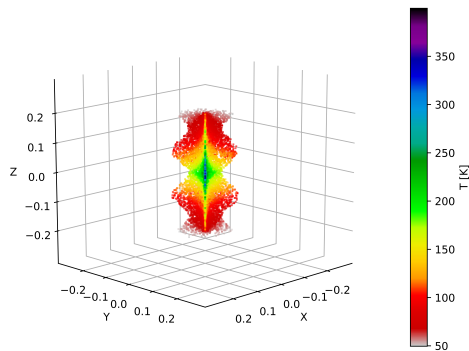


Fig. 1. Example of a customised sinusoidal, infalling, and rotating filament modelled with the `SF3DMODELS` package. The grid points are randomly distributed according to the density profile defined by the user. The colour map stands for the filament temperature.

instruments natively produce 3D or 4D data cubes with information on two position, one velocity/frequency, and optionally one polarization dimensions. Spectral cubes have typical resolutions in the range ~ 0.1 to a few km s^{-1} . Modern aperture-synthesis interferometers such as ALMA reach up to ~ 50 in the dynamic range of recovered angular scales and up to $> 10^3$ in peak S/N ¹.

The previous instrumental specifications have implications for modelling. Radio images that often were a simple ‘blob’ could be modelled reasonably well with homogeneous slabs or spheres, but resolved maps often cannot. ALMA and the expanded VLA are finding previously unknown multiplicity and features in almost every type of astrophysical source.

2. The SF3dmodels package

`SF3DMODELS` is a package that hosts physically-motivated analytical models, often used in star-formation research, but with wider applicability. Optionally, several individual *local* models can be put into a *global* model that is then

¹ <https://almascience.nrao.edu/documents-and-tools>

translated to the format of commonly used radiative-transfer codes, such as `LIME` (Brinch & Hogerheijde 2010), `POLARIS` (Reissl et al. 2018), or `RADMC-3D` (Dullemond et al. 2012) to produce synthetic images. Further analysis tools can pass these ‘perfect’ synthetic images through the instrument response to consider the effects of noise, spatial filtering, and angular resolution. `SF3DMODELS` is fully public and documented². If you find `SF3DMODELS` useful for your research, please cite Izquierdo et al. (2018).

2.1. The grid makers

Individual models from the library are created in *local grids*. As of August 2019, the model library includes: a variety of disk models based on a classical accretion disk prescription (Pringle 1981), but with flexibility to include piecewise density, temperature, and velocity fields; envelopes such as a modified Ulrich flow (Mendoza et al. 2004); generic turbulent spheres; cylindrical or parabolic filaments; jets as described in Reynolds (1986); and a variety of shapes matching those of observed ultracompact HII regions (De Pree et al. 2005). Additionally, the package allows the user to easily set simpler models such as uniform or power-law density and temperature distributions that might be useful when dealing with unresolved observations or benchmarks.

The grid cells in `SF3DMODELS` can be either cartesian with regular sampling or randomly distributed according to the gas properties. Often times, especially for high dynamic range problems, it is useful to better sample dense regions to resolve structures that contribute the most to the gas mass and focus the computational time accordingly during the radiative transfer. Moreover, models with complex geometries are easier to make up if random/non-regular grids are considered. Figure 1 shows the density-weighted 3D grid points distribution of a sinusoidal, infalling and rotating filament set up with the `FILAMENT` module of `SF3DMODELS` via an irregular mesh. The

² <https://star-forming-regions.readthedocs.io/en/latest/>

grid can trace any other gas property and particularly take advantage of the LIME capabilities to handle this type of grids for further radiative analysis.

Complex models can be created by adding several *local grids* into a *global grid*. The physical resolutions of these several grids can be different. If the sub-models overlap in 3D space, the average density in the corresponding cells is the mass-conserving average, the average temperature is the mass-weighted average, and the average velocity field is the mass-weighted vector average (Izquierdo et al. 2018).

2.2. The grid ingestors

Once the final model grid is created, it can easily be written into the format of LIME or RADMC-3D. LIME uses a non-homogeneous grid created from Delaunay triangulation (Brinch & Hogerheijde 2010), whereas RADMC-3D is cartesian with the option of Octree refinement (Dullemond et al. 2012). SF3D MODELS efficiently maps the model grid into the desired format for the ray-tracing within the radiative transfer code (Izquierdo et al. 2018). Input parameters for LIME or RADMC-3D can also be written by SF3D MODELS within a single Python script, so that the user does not need to fiddle with the particular format of input files in those packages.

We now summarize the first two applications of SF3D MODELS.

3. A complex model with radiative transfer for W33A MM1

W33A is a massive star-formation region known for its high bolometric luminosity and faint radio-continuum emission (Lin et al. 2016; van der Tak & Menten 2005). On parsec scales, filaments of dense molecular gas converge toward a central hub that hosts ongoing massive star formation (Galván-Madrid et al. 2010). Previous marginally resolved observations suggested the presence of a massive rotating disk/toroid with radius of a few $\times 1000$ au around a central (proto)star with mass $M_\star \sim 15 M_\odot$ (Galván-Madrid et al. 2010; Davies

et al. 2010). However, new ALMA observations changed this picture entirely. What was thought as a single object or binary, turned out to be a system with as many as 7 young stellar objects (YSOs). On top of that, this young stellar association or cluster is being fed by an accretion streamer (Maud et al. 2017).

The case for modelling this complex star-forming system was the main driver for the original development of SF3D MODELS. Figure 2 shows radiative transfer models of the (sub)mm CH_3CN lines for this source before (*leftmost* two columns) and after (*rightmost* three columns) the ALMA observations presented in Maud et al. (2017). The multiplicity of YSOs and gas streamers is also seen in other lines and dust continuum emission (Izquierdo et al. 2018; Maud et al. 2017). Thanks to the thorough modelling, we are able to extract useful information, as summarized below.

- There is an accretion filament or streamer feeding the fragmented core. The mass, length, and flow rate of this streamer are $M \sim 0.4 M_\odot$, $l \sim 7000$ au, and $\dot{M} \sim 5 \times 10^{-5} M_\odot \text{ yr}^{-1}$. Its short duty cycle ($t \sim 8000$ yr) suggests that either: *i*) we are witnessing a relatively late stage of accretion, *ii*) there is replenishment from larger scales, *iii*) the CH_3CN lines are only tracing a small fraction of the total infalling gas at these scales. Option *i* is disfavored when the weak ionization feedback is considered (weak cm continuum emission; van der Tak & Menten 2005), but is consistent with the current gas/star mass ratio at these scales $M_{\text{gas}}/M_\star \sim 0.1$ (Izquierdo et al. 2018). Option *ii* is suggested from the observational evidence for converging gas flows at multiple scales (Maud et al. 2017; Immer et al. 2014; Galván-Madrid et al. 2010). Regarding option *iii*, even if the gas kinematics are only inferred from (several) CH_3CN lines, the total gas mass is inferred also from modelling of the dust emission in two different wavelengths. Therefore, we discard this option at scales of a few $\times 1000$ au, although it could be correct at larger scales, which is related to option *ii*.

- There are accretion streamers joining some pairs of (proto)stars. Three of them are robust ‘detections’ from the modelling and two need confirmation. Their combined flow rate

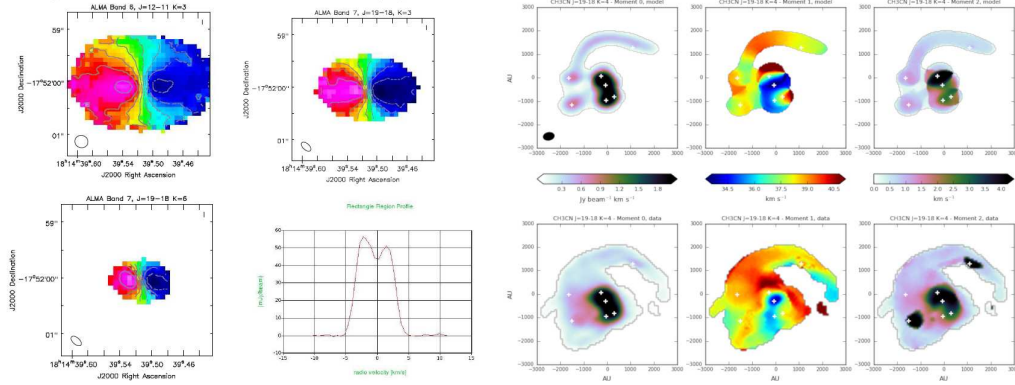


Fig. 2. *Leftmost* 2×2 columns and rows: previous radiative transfer modelling of CH_3CN line emission under the expectation of a single disk+envelope. The frames with color scale show the moment 1 map of different transitions at different energies and critical densities. The spectrum of one of them is also shown. *Rightmost* 3×2 columns and rows: the *bottom row* shows the new ALMA observations presented in Maud et al. (2017) and modelled in Izquierdo et al. (2018). The source breaks into several centers of star-formation activity and gas flows between them, plus one prominent gas streamer feeding the system. From *left to right* moment 0 (integrated line emission), moment 1 (‘mean’ velocity) and moment 2 (velocity dispersion). The *top row* shows the new multi-component model created with `SF3DMODELS`. The radiative transfer was calculated with LIME.

is $\dot{M} \sim 4 \times 10^{-5} M_{\odot} \text{ yr}^{-1}$, very close to that inferred for the larger, core-feeding streamer. Most of the accretion goes to sources Main and MNE. All this together suggests a hierarchical distribution of the accretion flows, dominated by the most massive source(s). This outcome is similar to that found in radiation-hydrodynamical simulations of gravitationally unstable star-forming cores (e.g., Krumholz et al. 2007).

- The stellar mass, rather than being concentrated in a single object, is distributed into several. There is still one massive (proto)star with $M_{\star} \approx 7 M_{\odot}$, which is also the most actively accreting. There are five other (proto)stellar sources with central masses in the range $M_{\star} \sim 0.6$ to $2.8 M_{\odot}$, plus one starless envelope. The total stellar ($M_{\text{stars}} \approx 11 M_{\odot}$) and gas mass ($M_{\text{gas}} \approx 1 M_{\odot}$) in the model are consistent with previous observations too.

- The dispersion of l.o.s. velocities of the (proto)stars in the model $\sigma_{v-\text{rms}} \approx 1.5 \text{ km s}^{-1}$ is very close to the 1D escape velocity from the model grid $v_{\text{esc}} \approx 1.3 \text{ km s}^{-1}$. The nascent stellar association appears to form in a quasi-virialized state. This is consistent with recent numerical simulations that show that virialized

(gas) cores fragment into more objects compared to sub-virial ones (Rosen et al. 2019).

4. On the effects of self-obscuration in class 0 protostellar disks

(Sub)millimeter spectral indices for dust continuum emission lower than the ISM value $\alpha \approx 3.7$ are usually interpreted as a signature of grain growth in – class II – protoplanetary disks (e.g., Carrasco-González et al. 2016). This is a most likely explanation, given that this continuum emission is almost always in the Rayleigh-Jeans limit ($h\nu \ll k_{\text{B}}T$) and believed to be optically thin. It is also a reasonable assumption because class II disks have had already $> 1 \text{ Myr}$ to evolve after the appearance of a protostar.

Class 0 YSOs represent the earliest stage of protostellar evolution, with a much larger mass reservoir and a much shorter evolutionary timescale compared to class II disks (e.g., Evans et al. 2009). Recently, dust spectral indices $\alpha \approx 2$ to 3.5 have been systematically found in class 0 protostars at disk scales. Their interpretation has sometimes also been in terms of dust evolution (e.g., Miotello et al.

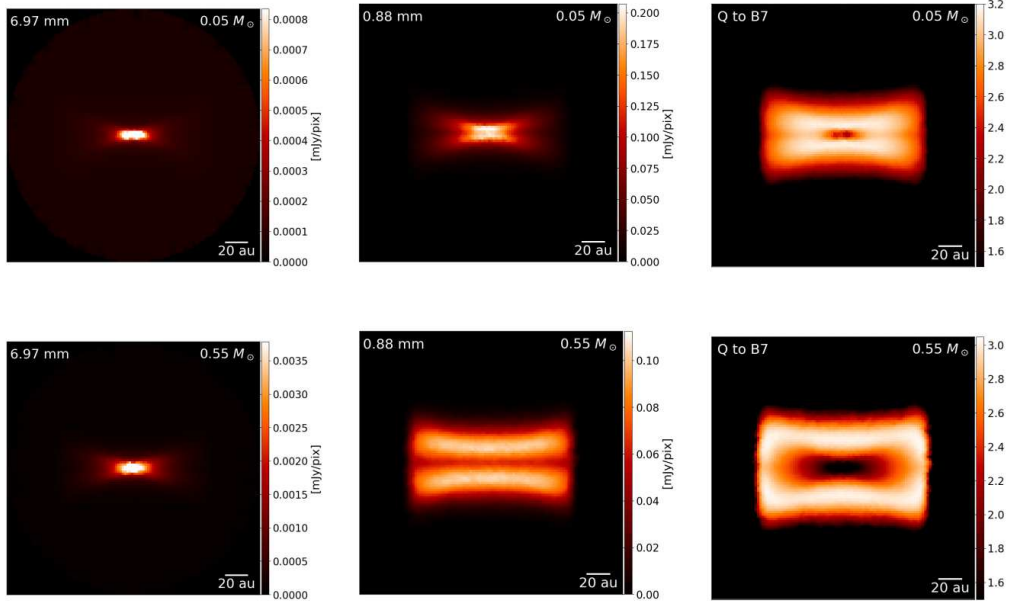


Fig. 3. *Top and bottom rows show disk model images with $M = 0.05 M_{\odot}$ and $M = 0.55 M_{\odot}$, respectively. From left to right, panels show a synthetic image a 7 mm (VLA Q band), 0.8 mm (ALMA Band 7) and the resolved spectral index between these bands. Taken from Galván-Madrid et al. (2018).*

2014). Li et al. (2017) showed that a simple two-temperature model with a hot, relatively massive region inside a colder, also massive one was enough to reproduce the low (sub)mm spectral indices in their class 0 disk sample. In their interpretation, the hot, inner component – the inner disk – is hidden at all frequencies > 100 GHz, and only starts contributing to the observed flux at lower frequencies, thus flattening the spectral index. More recently, Lee et al. (2017) presented astonishing ALMA images of an edge-on protostellar disk with 8 au resolution which show a prominent dark lane. This characteristic ‘hamburger’ morphology proves the existence of self-obscuration at (sub)mm wavelengths in at least this particular object.

We used SF3D MODELS and LIME to systematically explore the hypothesis that low spectral indices observed in protostellar disks are mainly caused by self-obscuration within a density and temperature gradient. These results were reported in Galván-Madrid et al. (2018).

First, we found a fiducial model that reproduces within a few percent the reported flux of

the Lee et al. (2017) ‘hamburger’ at 0.8 mm, as well as size, and ‘bun’ contrast. Then we created several grids of models to explore the parameter space and see under which conditions we get low dust continuum spectral indices. We varied disk mass, viewing angle, and observing frequency, as well as the dust opacity β index³. In total, our grids consist of 16616 model images. These images were resampled and fitted using the same observing bands and noise levels as in the sample of Li et al. (2017). The main results are described below (for more details, see Galván-Madrid et al. 2018).

- Self-obscuration in protostellar disks with a temperature gradient has important effects in their appearance, most notably the existence of dark lanes. These become more prominent with increasing mass, observing frequency, and viewing angle closer to edge-on.

- Source-integrated spectral indices tend to be significantly smaller than the optically-thin ISM value $\alpha_{\text{ISM}} \approx 3.7$. We conclude that all

³ $\alpha = \beta + 2$ in the Rayleigh-Jeans, optically thin limit.

ALMA bands are significantly affected for all models with $M > 0.05 M_{\odot}$, regardless of inclination.

- Determinations of protostellar disk masses could often be underestimated by factors larger than 10. Observations at $\nu < 50$ GHz could be the key to have better measurements of protostellar disk masses.

5. Future work

We are currently using SF3DMODELS to model free-free and recombination line emission with RADMC-3D (Peters et al. 2012) in several projects with new ALMA and VLA data. We also plan to further contribute to the science case of a Next Generation VLA (Galván-Madrid et al. 2018b). We look forward to have more users for SF3DMODELS within and beyond close collaborations.

Acknowledgements. RGM and AFI acknowledge support from UNAM-PAPIIT Programme IN104319. We are grateful to Luke Maud and Adam Ginsburg for hosting AFI at several stages of the development of SF3DMODELS.

References

- Brinch, C., & Hogerheijde, M. R. 2010, *A&A*, 523, A25
- Carrasco-González, C., Henning, T., Chandler, C. J., et al. 2016, *ApJ*, 821, L16
- Davies, B., Lumsden, S. L., Hoare, M. G., et al. 2010, *MNRAS*, 402, 1504
- De Pree, C. G., Wilner, D. J., Deblasio, J., et al. 2005, *ApJ*, 624, L101
- Dullemond, C. P., Juhasz, A., Pohl, A., et al. 2012, RADMC-3D: A multi-purpose radiative transfer tool, *ascl:1202.015*
- Evans, N. J., Dunham, M. M., Jørgensen, J. K., et al. 2009, *ApJS*, 181, 321
- Galván-Madrid, R., Zhang, Q., Keto, E., et al. 2010, *ApJ*, 725, 17
- Galván-Madrid, R., Liu, H. B., Izquierdo, A. F., et al. 2018, *ApJ*, 868, 39
- Galván-Madrid, R., Beltrán, M., Ginsburg, A., et al. 2018b, Science with a Next Generation Very Large Array, 309
- Immer, K., Galván-Madrid, R., König, C., et al. 2014, *A&A*, 572, A63
- Izquierdo, A. F., Galván-Madrid, R., Maud, L. T., et al. 2018, *MNRAS*, 478, 2505
- Krumholz, M. R., Klein, R. I., & McKee, C. F. 2007, *ApJ*, 665, 478
- Lin, Y., Liu, H. B., Li, D., et al. 2016, *ApJ*, 828, 32
- Lee, C.-F., Li, Z.-Y., Ho, P. T. P., et al. 2017, *Science Advances*, 3, e1602935
- Li, J. I.-H., Liu, H. B., Hasegawa, Y., et al. 2017, *ApJ*, 840, 72
- Mendoza, S., Cantó, J., & Raga, A. C. 2004, *Rev. Mex. Astron. Astrofis.*, 40, 147
- Maud, L. T., Hoare, M. G., Galván-Madrid, R., et al. 2017, *MNRAS*, 467, L120
- Miotello, A., Testi, L., Lodato, G., et al. 2014, *A&A*, 567, A32
- Offner, S. S. R., Lee, E. J., Goodman, A. A., et al. 2011, *ApJ*, 743, 91
- Peters, T., Longmore, S. N., & Dullemond, C. P. 2012, *MNRAS*, 425, 2352
- Pringle, J. E. 1981, *ARA&A*, 19, 137
- Reissl, S., Wolf, S., & Brauer, R. 2018, POLARIS: POLARized Radiation Simulator, *ascl:1807.001*
- Reynolds, S. P. 1986, *ApJ*, 304, 713
- Rosen, A. L., Li, P. S., Zhang, Q., et al. 2019, arXiv e-prints, [arXiv:1902.10153](https://arxiv.org/abs/1902.10153)
- Smith, R. J., Glover, S. C. O., Klessen, R. S., et al. 2016, *MNRAS*, 455, 3640
- van der Tak, F. F. S., & Menten, K. M. 2005, *A&A*, 437, 947
- van der Tak, F. F. S., Black, J. H., Schöier, F. L., et al. 2007, *A&A*, 468, 627